Oxidative steam reforming of methane over Ni/α-Al_2O_3 modified with trace Pd

*Kaori Yoshida[a], Kazu Okumura[b], Toshihiro Miyao[c], Shuichi Naito[c], Shin-ichi Ito[a], Kimio Kunimori[a], Keiichi Tomishige[a]**

[a] *Institute of Materials Science, University of Tsukuba, 1-1-1 Tennodai, Tsukuba, Ibaraki 305-8573, Japan*

[b] *Department of Materials Science, Faculty of Engineering, Tottori University, Koyama-cho Minami, Tottori 680-8552, Japan*

[c] *Department of Applied Chemistry, Faculty of Engineering, Kanagawa University, 3-27-1, Rokkakubashi, Kanagawa-ku, Yokohama, Kanagawa 221-8686, Japan*

Corresponding author

Keiichi Tomishige
Institute of Materials Science, University of Tsukuba
1-1-1 Tennodai, Tsukuba, Ibaraki 305-8573, Japan
Tel/Fax: +81-29-853-5030
E-mail: tomi@tulip.sannet.ne.jp

Abstract

Ni catalysts supported on α-Al_2O_3 modified with small amounts of Pd were prepared by different impregnation methods to investigate catalytic performance and catalyst bed temperature profile in oxidative steam reforming of methane. The Pd+Ni bimetallic catalysts prepared by the co-impregnation method showed higher resistance to hot-spot formation than monometallic Ni and bimetallic Pd/Ni catalysts prepared by two sequential impregnations, in particular, Pt+Ni catalysts prepared by the co-impregnation method. The additive effect of Pd on the Pd/Ni catalysts was discussed on the bases of metal particle size and structural analysis by Pd *K*-edge extended X-ray absorption fine structure.

Graphical Abstract

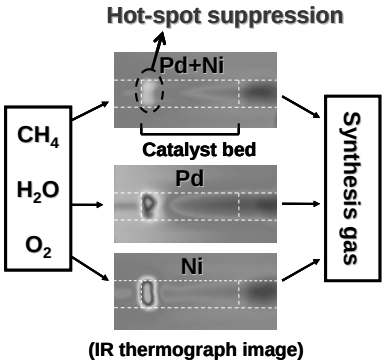

The Pd+Ni bimetallic catalysts supported on α-Al_2O_3 prepared by a co-impregnation method are much more effective for the suppression of hot-spot formation in oxidative steam reforming of methane than the corresponding monometallic catalysts, which is caused by synergy between Pd with high reducibility and Ni with high reforming activity.

Keywords: oxidative reforming, steam reforming, methane, Ni, Pd, Pt, thermography, hot spot, co-impregnaiton.

1. Introduction

Oxidative steam reforming of methane is a promising method for an energy-efficient syngas production from natural gas [1]. Oxidative steam reforming of methane is the combination of methane steam reforming (Eq. (1)) with methane combustion (Eq. (2)); the partial pressure of the reactants is adjustable to autothermal conditions. However, oxidative steam reforming of methane has a problem of hot-spot formation at the catalyst bed inlet, which is a common problem in the reforming of hydrocarbons using oxygen. Noble metal catalysts such as Rh and Pt have been reported to be effective for the suppression of hot-spot formation [2, 3]. In contrast, Ni catalysts usually tend to form hot spots at the catalyst bed inlet in the presence of gas-phase oxygen [4–6].

$CH_4 + H_2O \rightarrow CO + 3H_2 \quad \Delta H^0_{298\,K} = +206\ kJ \cdot mol^{-1}$ (1)

$CH_4 + 2O_2 \rightarrow CO_2 + 2H_2O \quad \Delta H^0_{298\,K} = -803\ kJ \cdot mol^{-1}$ (2)

Considering the high cost and limited availability of noble metals, the main component should be nickel. Therefore, our group has been developing Ni-based catalysts modified with a small amount of noble metal for oxidative reforming of methane with high resistance to hot-spot formation [7–12]. Here, one strategy is the combination of high reducibility of noble metals with high reforming activity of Ni. The Pt-Ni and Pd-Ni bimetallic catalysts supported on γ-Al_2O_3 were investigated and the relation between the structure of bimetallic particles and the resistance to hot-spot formation in oxidative reforming of methane has been reported [7–12]. Here, we tested the bimetallic catalysts supported on α-Al_2O_3 with larger Ni loading amount, which will be more applicable to a practical process. In particular, the effect of preparation methods on catalytic performance and the temperature profile of the catalyst bed in oxidative steam reforming of methane over Pd-Ni and Pt-Ni bimetallic catalysts were investigated. In addition, catalysts were characterized by the measurement of H_2 adsorption amount, temperature-programmed reduction (TPR), transmission electron microscopy (TEM), and extended X-ray absorption fine structure (EXAFS). The relation between the structure of bimetallic particles and the catalytic performance in oxidative steam reforming of methane is also discussed.

2. Experimental Section

2.1. Catalyst preparation

An alumina support was prepared by the calcination of JRC-ALO-1 (provided by Catalysis Society of Japan, S_{BET} =143 $m^2 \cdot g^{-1}$, grain size of 2–3 mm) in air at 1423 K for 3 h. After the calcination, the microstructure was changed from γ-Al_2O_3 to α-Al_2O_3, which was confirmed by X-ray diffraction. The surface area of the calcined alumina was determined to be 8 m^2/g. It was crushed and sieved to particle sizes between 180–250 μm before impregnation. Supported monometallic Ni catalysts were prepared by an impregnation method using an aqueous solution of $Ni(NO_3)_2 \cdot 6H_2O$ (99.9%, Wako Pure Chemical Industries Ltd.), $Ni(CH_3COO)_2 \cdot 4H_2O$ (99.9%, Kanto Chemical Co., Inc.) and $NiCl_2 \cdot 6H_2O$ (99.9%, Soekawa Chemical Co., Ltd.). Supported monometallic Pd and Pt catalysts were prepared by an impregnation method using an aqueous solution of $PdCl_2$ (99.9%, Soekawa Chemical Co., Ltd.) and $H_2PtCl_6 \cdot 6H_2O$ (99.9%, Soekawa

Chemical Co., Ltd.). After removal of the solvent by heating and evaporation at 353 K, the resulting product was dried in an oven at 383 K for 12 h. Subsequently, the sample was calcined at 773 K in air for 3 h. Bimetallic catalysts (Pd-Ni and Pt-Ni) were prepared by using sequential impregnation and co-impregnation methods. In particular, two different sequential methods were applied. In the case of the sequential impregnation methods, the calcined monometallic nickel catalyst was reduced at 1123 K for 0.5 h under H_2 flow, and then this treated sample was impregnated again under air atmosphere. In one sequential impregnation method, the acetone solution of $Pd(C_5H_7O_2)_2$ (99.9%; Soekawa Chemical Co., Ltd.) or $Pt(C_5H_7O_2)_2$ (99.9%; Soekawa Chemical Co., Ltd.) was used as a precursor. After removal of the acetone solvent, the catalyst was dried at 383 K for 12 h and calcined in air at 573 K for 3 h. In the other sequential impregnation method, the aqueous solution of $PdCl_2$ was used as a precursor. After the solvent removal, the catalyst was dried at 383 K and calcined in air at 773 K. We also prepared the catalysts by the co-impregnation method, where the precursor is a mixed aqueous solution of $Ni(NO_3)_2{\cdot}6H_2O$ + $PdCl_2$ or $Ni(NO_3)_2{\cdot}6H_2O$ + $H_2PtCl_6{\cdot}6H_2O$. After co-impregnation, the preparation procedure is identical to that of the monometallic Ni catalyst. Table 1 lists the catalysts prepared in this study. The notation of the catalysts is specified in Table 1.

2.2. Activity test and thermographical observation

Oxidative steam reforming of methane was conducted under atmospheric pressure in a fixed-bed quartz reactor (i.d. 3 mmϕ, o.d. 5 mmϕ). The temperature profile of the catalyst bed was measured using infrared thermograph equipment (TH31; NEC San-ei Instruments Ltd.) in the same method as previously reported [11]. The catalyst (0.045 g) was reduced in the hydrogen flow (30 $ml{\cdot}min^{-1}$, 100% H_2) at 1123 K for 0.5 h in the reactor. After reduction, the feed gases (the mixture of CH_4, O_2, steam and Ar) were introduced to the catalyst bed at various contact times W/F (W(g) = catalyst weight, F($mol{\cdot}h^{-1}$) = total flow rate of gases). Gases such as CH_4, O_2, H_2 and Ar used here were research grade; they were obtained from Takachiho Trading Co. Ltd. The gases were used without further purification. Steam was obtained by vaporizing distilled water that was supplied using a feeding pump (MT2111, Moleh Ltd.). The partial pressure ratio of the feeding gases is $CH_4/H_2O/O_2/Ar$ = 40/30/20/10. An iced water trap was located at the reactor exit to remove the steam contained in the effluent gas. The gas was collected from the sampling port using a micro-syringe. Then it was analyzed using a gas chromatograph (GC-14A; Shimadzu Corp.) equipped with a flame ionization detector (FID) and a thermal conductivity detector (TCD). Concentrations of CO, CO_2 and CH_4 in the effluent gas were determined using an FID-GC equipped with a methanator and a stainless steel column packed with Gaskuropack 54 (GL Science). The H_2 concentration was determined using TCD-GC with a stainless steel column packed with a molecular sieve 13X. Methane conversion and CO selectivity in oxidative steam reforming of methane were calculated as described below:

$$\text{Methane conversion } (\%) = \frac{C_{CO} + C_{CO_2}}{C_{CH_4} + C_{CO} + C_{CO_2}} \times 100,$$

$$\text{CO selectivity (\%)} = \frac{C_{CO}}{C_{CO} + C_{CO_2}} \times 100 ,$$

where C is the concentration of each gas in the effluent gas.

The amount of deposited coke during the reaction was able to be neglected in all the cases presented here, although coke deposition has often been observed in methane reforming [14–16].

2.3. Catalyst characterization

The fresh catalysts were characterized by a chemisorption experiment, which was carried out in a high-vacuum system by volumetric methods (dead volume: 65 cm^3). Prior to the adsorption measurement, the catalysts were reduced in flowing H_2 at 1123 K for 0.5 h in the fixed-bed reactor, which was used in the activity test. The pre-treated catalyst was transferred to the measurement cell in air, and the cell was connected to the vacuum line. The H_2 reduction at 773 K for 0.5 h and evacuation at 723 K for 1 h were carried out. After the pretreatments, the adsorption amount of H_2 was measured at room temperature; the equilibrium pressure was about 2.7 kPa.

Temperature programmed reduction (TPR) profiles were measured in a fixed bed quartz reactor. Each time, 0.03 g of sample was loaded into the quartz reactor and heated with a heating rate of 10 $K \cdot min^{-1}$, from room temperature to 1123 K in 5% hydrogen diluted in argon (30 $ml \cdot min^{-1}$) as a reducing gas. Water that formed during the reduction was removed using a cold trap with frozen acetone (ca. 173 K). The TPR profile was monitored continuously with an on-line TCD-GC. The H_2 consumption was estimated from the integrated peak area in the reduction profiles.

Transmission electron microscope (TEM) images were taken by means of JEM-2010F (JEOL) equipment operated at 200 kV. First, the catalysts were reduced by H_2 pretreatment at 1123 K for 0.5 h in a fixed bed reactor. After this reduction, samples were stored under N_2 until the measurements. Samples were dispersed in 2-propanol using supersonic waves. They were put on Cu grids for TEM observation under air atmosphere. The average particle size of metal particles is calculated using the equation below [17]:

$$d = \sum_i n_i d_i^{\,3} / \sum_i n_i d_i^{\,2} ,$$

where n_i is the number of the particles and d_i is the characteristic diameter of the particles.

The Pd *K*-edge and Pt L_3-edge extended X-ray absorption fine structure (EXAFS) were measured at the BL01B1 station in the SPring-8 with the approval of the Japan Synchrotron Radiation Research Institute (JASRI) (Proposal No. 2006A1058). The storage ring was operated at 8 GeV. A Si(111) single crystal was used to obtain a monochromatic X-ray beam. Two ion chambers filled with 50% Ar + 50% N_2 and 75% Ar + 25% Kr were used as detectors of I_0 and I, respectively. The sample weight was 0.55 g and 0.04 g for Pd *K*-edge and Pt L_3-edge EXAFS, respectively. The catalysts were treated by H_2 at 1123 K for 0.5 h in a fixed-bed reactor and the samples were pressed into self-supporting 7-mm-diameter wafers under atmosphere, followed by the treatment again with H_2 at 773 K for 0.5 h in the cell. After this pretreatment, each sample was transferred to the measurement cell using a glove box filled with nitrogen to prevent exposure of the sample disk to air. The thickness of the sample disk was about 6 mm and 0.5 mm to give 0.10 and 0.06 edge jump

for the Pd *K*-edge and Pt L_3-edge EXAFS, respectively. EXAFS data were collected in a transmission mode at room temperature. For EXAFS analyses, the oscillation was first extracted from EXAFS data using a spline smoothing method [18]. The oscillation was normalized by the edge height around 50 eV. The Fourier transformation of the k^3-weighted EXAFS oscillation from *k* space to *r* space was performed to obtain a radial distribution function. The inversely Fourier filtered data were analyzed using a usual curve fitting method [19, 20]. The Fourier transform and Fourier filtering ranges are shown for each result. For the curve fitting analysis, the empirical phase shift and amplitude functions for the Pd-Pd and Pt-Pt bonds were extracted respectively from Pd and Pt foils. Theoretical functions for the Pd-Ni and Pt-Ni bonds were calculated using the FEFF8.2 program [21]. Analyses of EXAFS data were performed using the "REX2000" program (Version: 2.3.3; Rigaku Corp.).

3. Results and Discussion

3.1. Catalytic performance and catalyst bed temperature profile in oxidative steam reforming of methane

The catalytic performance in terms of the methane conversion, H_2/CO ratio and CO selectivity over Ni(N, 10.6) and Pd(C, 0.07) are listed in Table 2, entries 1 and 2. Methane conversion over Ni(N, 10.6) was as high as that at the reaction equilibrium even at low *W*/*F* values such as 0.04 gh/mol. In contrast, Pd(C, 0.07) gave much lower methane conversion even when *W*/*F* was higher. This result is related to the small loading amount of Pd and the low catalytic activity of Pd in oxidative steam reforming [3]. Figures 1 (A) and (B) show the effect of *W/F* on the catalyst bed temperature profile over Ni (N, 10.6) and Pd(C, 0.07), respectively. The exothermic profile near the catalyst bed inlet was observed and the temperature increased with decreasing *W*/*F* on both catalysts. The temperature on Ni(N, 10.6) reached about 1350 K at *W*/*F* = 0.04 gh/mol (Table 2, entry 1). This behavior can be explained by separation of the reaction zones for combustion and reforming in oxidative steam reforming of methane, as reported previously [10]. In the presence of gas-phase oxygen near the catalyst bed inlet, the Ni species is oxidized and is active only for methane combustion, which increased the catalyst bed temperature drastically. On the other hand, in the absence of gas-phase oxygen, the Ni species is maintained in a metallic state and is active for methane reforming, which decreased the catalyst bed temperature remarkably. The separation of the reaction zones causes the large temperature gradient in the catalyst bed. In the case of Pd(C, 0.07), the large temperature gradient can be explained by high combustion activity and low reforming activity. As a result, we can conclude that the monometallic Ni and Pd catalysts are not suitable for the oxidative steam reforming of methane because of hot-spot formation. The catalytic performance and temperature profile of Pd(C, 0.07)+Ni(N, 10.6) are also shown in Table 2, entry 3, and in Figure 1(C). Pd(C, 0.07)+Ni(N, 10.6) showed high methane conversion like Ni(N, 10.6) and gave a much flatter temperature profile than Pd(C, 0.07) and Ni(N, 10.6). This result indicates that the synergy between Pd and Ni decreases the bed temperature and suppresses the hot-spot formation. According to our previous reports, the catalytic performance and bed temperature profile on bimetallic catalysts in oxidative steam reforming of methane are strongly influenced by the structure of

bimetallic particles and by the preparation method [7–12]. Therefore, catalysts prepared by different methods were evaluated in oxidative steam reforming of methane. Table 2 lists the catalytic performance in oxidative steam reforming of methane over various Pd-Ni bimetallic catalysts. In the case of 0.07 wt% Pd-10.6 wt% Ni(N) bimetallic catalysts, all these catalysts gave high methane conversion; however, the order of the highest bed temperature was as follows: Pd(A, 0.07)/Ni(N, 10.6) > Pd(C, 0.07)/Ni(N, 10.6) > Pd(C, 0.07)+Ni(N, 10.6) (Table 2, entries 3–5). A similar tendency was observed over 0.2 wt% Pd-10.6 wt% Ni(N) bimetallic catalysts (Table 2, entries 6–8). In particular, from a comparison between Pd(C, 0.07)+Ni(N, 10.6) and Pd(C, 0.2)+Ni(N, 10.6) (Table 2, entries 3 and 6), it is found that excess Pd can enhance the highest bed temperature, probably due to the high combustion activity of Pd.

As reported previously, the addition of Pt was effective to the suppression of hot-spot formation [3]. Therefore, we also investigated the performance of bimetallic Pt-Ni and monometallic Pt catalysts (Table 2, entries 9–12). Here, the molar loading amounts of 0.14 wt% and 0.4 wt% Pt correspond to those of 0.07 wt% and 0.2 wt% Pd. In the case of Pt-Ni bimetallic catalysts, the co-impregnation method was also effective. Another interesting point is that Pd is a more effective additive than Pt at the same molar amount, although the monometallic Pt catalyst was much more effective than the monometallic Pd catalyst (Table 2, entries 2 and 9). This indicates that the additive effect of noble metals on the co-impregnation bimetallic catalysts cannot be caused by their own reforming activity. Figure 2 shows the reaction time dependence in oxidative steam reforming of methane over Pd(C, 0.07)+Ni(N, 10.6), and it is found that the catalytic performance was stable during 8 h.

3.2. Catalyst characterization

The amount of H_2 adsorption and the particle size calculated on the basis of the H_2 adsorption data are also listed in Table 1. Figure 3 shows the TEM images of the catalysts after H_2 reduction. The obtained average particle sizes of reduced catalysts by TEM observation are also listed in Table 1. The particle size determined by TEM agreed well with that based on H_2 adsorption data. The average metal particle size is strongly influenced by the preparation method. It was clear that the catalysts prepared by the co-impregnation method gave higher metal dispersion than the catalysts prepared by two sequential impregnation methods or the monometallic Ni catalyst. In contrast, the catalysts prepared by the sequential impregnation using $PdCl_2$ and $Pd(acac)_2$ gave larger average particle sizes than the monometallic Ni catalyst.

Here, the relation between the highest bed temperature in oxidative steam reforming of methane and the average particle size is shown in Figure 4. In particular, in order to evaluate the particle size of monometallic Ni catalysts, we prepared and tested the Ni catalysts with different precursors, because it has been reported that different precursors brought about different metal dispersion values [22]. The data of Ni(Ac, 10.6) and Ni(C, 10.6) are listed in Tables 1 and 2, entries 14 and 15. The highest bed temperature is clearly influenced by the particle size. In the case of monometallic Ni catalysts, the temperature increased with increasing average particle size monotonously. This tendency was observed on almost all the bimetallic catalysts. The addition of Pd is totally effective to create the decrease of the highest bed temperature. The preparation method

and the precursor which gave smaller particle size were more effective in the suppression of hot-spot formation. In the case of the Pd-Ni bimetallic catalysts, it is characteristic that the larger amount of Pd addition increased the particle size and the highest bed temperature. In contrast, the co-impregnation Pt-Ni catalysts showed different tendencies from the case of Pd. The Pt(C, 0.2)+Ni(N, 10.6) gave higher bed temperature than Pt(C, 0.07)+Ni(N, 10.6), and this is related to smaller particle size of Pt(C, 0.2)+Ni(N, 10.6) than that of Pt(C, 0.07)+Ni(N, 10.6). Unlike the case of Pd, it is characteristic that large amount of Pt addition decreased particle size and the highest bed temperature. In addition, here, the relation between the highest bed temperature and the average particle size of fresh catalysts was described. The observed good relation suggests that the particle size can be unchanged during the reaction, which is also supported by the stability of catalytic performance in the activity test for longer reaction time, as shown in Figure 2.

Figure 5 shows the temperature-programmed reduction (TPR) profiles of Ni(N, 10.6), Pd(C, 0.2)+Ni(N, 10.6), Pd(C, 0.2)/Ni(N, 10.6), Pd(A, 0.2)/Ni(N, 10.6) and reference catalysts. The reduction of the Ni species on Ni(N, 10.6) proceeded in the temperature range of 623–923 K, and the total amount of H_2 consumption agrees with the stoichiometry of $NiO + H_2 \rightarrow Ni + H_2O$. This agreement means that all the Ni species are present in the oxidized state and they are reduced to Ni metal. In the case of Pd(C, 0.2)+Ni(N, 10.6), the H_2 consumption peak was shifted to lower temperature and the addition of Pd promoted the reduction of the Ni species. On Pt(C, 0.4)+Ni(N, 10.6), the peak was shifted to much lower temperature. The addition of Pt also promoted the reduction, an the promoting effect of Pt was more remarkable than that of Pd. This behavior is caused by hydrogen spilt-over from noble metals to Ni species [23, 24]. On the other hand, in case of Pd(C, 0.2)/Ni(N, 10.6) and its reference catalyst (Ni(N, 10.6)-calcined at 773 K after the reduction at 1123 K), the total amount of H_2 consumption was 82–86 %. This indicates that a part of the Ni species are present in a metallic state after the calcination at 773 K. This tendency was more remarkable on Pd(A, 0.2)/Ni(N, 10.6) and its reference catalyst (Ni(N, 10.6)-calcined at 573 K after the reduction at 1123 K). In all the cases, addition of Pd to the Ni catalysts promotes the reduction of Ni species. However, the reducibility of the catalyst is not directly related to the suppression of hot-spot formation. Therefore, the local structure from the viewpoint of the additives was compared by the EXAFS analysis.

Figure 6 shows Pd *K*-edge EXAFS results of Pd(C, 0.2)+Ni(N, 10.6), Pd(C, 0.2)/Ni(N, 10.6) and Pd(A, 0.2)/Ni(N, 10.6) after H_2 reduction. The curve fitting results are listed in Table 4. Both Pd-Ni and Pd-Pd bonds are demanded for good curve fitting results. The length of the Pd-Pd bond of the catalysts is a little shorter than that in Pd foil, and the lengths of the Pd-Pd and Pd-Ni bonds agreed well with those in the previous reports [11, 12, 25–29]. The agreement suggests the formation of Pd-Ni alloy with high Ni content. The Pd atoms can partially substitute Ni atoms in Ni metal crystallite. In addition, when Pd and Ni are well mixed in the alloy phase, the CN ratio of the Pd-Pd to Pd-Ni bonds must be close to its composition (molar ratio of Pd to Ni on Pd(C, 0.2)+Ni(N, 10.6) = 0.01). However, the obtained CN ratio of the Pd-Pd to Pd-Ni bonds was much higher than the composition. Therefore, it is thought that Pd can be segregated in the alloy. Furthermore, another important point is that the sum of the CNs of the Pd-Pd and Pd-Ni bonds on Pd(C,

0.2)+Ni(N, 10.6), Pd(C, 0.2)/Ni(N, 10.6) and Pd(A, 0.2)/Ni(N, 10.6) were 9.1, 9.6 and 10.5, respectively. These values are smaller than the CN of the bulk Pd atom in Pd foil, and we interpreted the smaller CN values as due to the Pd atoms near the surface. The results suggest that the order of the ratio of the surface Pd atoms is as follows: Pd(C, 0.2)+Ni(N, 10.6) > Pd(C, 0.2)/Ni(N, 10.6) > Pd(A, 0.2)/Ni(N, 10.6). This tendency can be connected to the average metal particle size as listed in Table 1. The catalysts with larger metal particles gave higher coordination numbers of the Pd-Pd and Pd-Ni bonds. The particle sizes on Pd(A, 0.2)/Ni(N, 10.6) and Pd(C, 0.2)/Ni(N, 10.6) were larger than that on Ni(N, 10.6). Although the details are not shown here, the metal particles were not so aggregated by the same preparation procedure when Pd was not added. Therefore, it is thought that the aggregation is not due to the preparation procedure for the sequential impregnation, but due to the presence of Pd. As reported previously, the noble metal atoms such as Pd and Pt introduced by the sequential impregnation method tend to be present near the surface on Ni metal particles [10, 11]. In these reported cases, the aggregation induced by noble metal addition was not so significant, probably because the support was γ-Al_2O_3 and the metal particle size was much smaller. In contrast, in the present case, α-Al_2O_3 was used as a support and the metal particle size was large; here the concentration of Pd on the surface during the reduction can be relatively high, and too high surface Pd concentration over bimetallic particles can cause the aggregation of metal particles. In addition, the surface Pd atoms before the aggregation can be incorporated into the bulk of aggregated metal particles.

In contrast, the Pd(C, 0.07)+Ni(N, 10.6) and Pd(C, 0.2)+Ni(N, 10.6) catalysts prepared by co-impregnation method had smaller metal particles than the monometallic Ni(N, 10.6). Since the noble metal atoms introduced by the co-impregnation are not preferentially located on the surface of the particles, the surface concentration of noble metal atoms cannot be so high. This is why the addition of Pd by the co-impregnation method did not cause the aggregation of metal particles. However, the mechanism of the promoting effect of the Pd addition on higher dispersion is not elucidated and further investigations are necessary.

Another important point is that Pd(C, 0.2)+Ni(N, 10.6) was more effective than Pt(C, 0.4)+Ni(N, 10.6). Considering that the metal particle size of Pd(C, 0.2)+Ni(N, 10.6) was larger than that of Pt(C, 0.4)+Ni(N, 10.6), we conclude that Pd is a more effective additive than Pt. Based on the Pt L_3-edge EXAFS (Table 3), the bond lengths of Pt-Pt and Pt-Ni were much shorter than that of the intermetallic compound between Pt and Ni (NiPt and Ni_3Pt) [30]. This indicates that the intermetallic compounds are not formed, but Pt-Ni alloy phase is formed. This behavior is supported by previous reports [9, 31–33]. The coordination number of the Pt-Ni bond was much larger than that of the Pt-Pt bond on Pt(C, 0.4)+Ni(N, 10.6). This suggests that Pt atoms are incorporated to Ni metal crystallite in more isolated locations. On the other hand, the coordination number of the Pd-Ni bond was smaller than that of the Pd-Pd bond on Pd(C, 0.2)+Ni(N, 10.6), which is opposite to the case of Pt(C, 0.4)+Ni(N, 10.6). The higher coordination number of the Pd-Pd bonds and the smaller sum of coordination number of the Pd-Pd and Pd-Ni bonds suggest that small Pd clusters or islands are formed near the surface in the bimetallic particles.

3.3. Difference between Pd and Pt on the bimetallic catalysts

High catalyst temperature at the bed inlet has been observed over Ni catalysts in oxidative steam reforming of methane [4–6]. This phenomenon is explainable by the separation of combustion and reforming reaction zones. In contrast, the modification of Ni particles with noble metals such as Pd and Pt has been reported to be effective for the suppressing of the temperature gradient and hot-spot formation [7–12]. This effect can be related to the oxygen affinity of Pd and Pt being much lower than that of Ni [34]. The intimate interaction of Ni with noble metal atoms enables the maintenance of the metallic state of Ni even in the presence of gas-phase oxygen, and the reforming reactions can proceed even in the catalyst bed inlet, along with the combustion reaction. The overlap between the endothermic and the exothermic reaction zones can give flatter catalyst bed temperature and can suppress hot-spot formation.

On the monometallic Ni catalysts, the highest bed temperature in the oxidative steam reforming of methane slightly increased with increasing metal particle size, probably because of higher combustion activity on larger particles. On the other hand, the addition of Pd and Pt by co-impregnation method was also effective for the suppression of the hot-spot formation. One reason is to decrease the average particle size. The other is to suppress the oxidation of Ni and to overlap the reaction zones. An interesting point is that Pd is comparable or superior to Pt in the positive effect, although the monometallic Pd catalyst showed higher combustion activity and lower reforming activity than the monometallic Pt catalyst. The results of the monometallic catalysts suggest that Pt is a much more suitable modifier than Pd.

Unlike the monometallic Pd catalyst, the combustion activity of Pd(C, 0.2)+Ni(N, 10.6) can not be so high. This property is caused by very small Pd clusters or surface islands on the bimetallic particles. If the high combustion activity of Pd itself can be suppressed, Pd can be an effective additive because of low oxygen affinity and high reducibility. In addition, the coordination number ratio of the M-M bond to the M-Ni bond (M = Pd, Pt) in the EXAFS analysis can represent the interaction of M with Ni and the solubility of M to Ni. Strong interaction of Pt with Ni and high solubility of Pt to Ni can decrease the surface concentration of Pt on the bimetallic particles. The opposite property of Pd can increase the surface concentration of Pd to some extent, which can make Pd an excellent modifier in the oxidative steam reforming.

4. Conclusions

1. Catalyst bed temperature profiles were measured in oxidative steam reforming of methane ($CH_4/H_2O/O_2/Ar$ = 40/30/20/10) over α-Al_2O_3 supported bimetallic Pd-Ni catalysts prepared by different methods; we compared monometallic Ni catalysts, Pt-Ni bimetallic catalysts, monometallic Pd and Pt catalysts. Pd+Ni catalysts prepared by a co-impregnation method was more effective in the suppression of hot-spot formation than Pd/Ni catalysts prepared by two sequential impregnation methods and monometallic Ni catalysts. Another interesting point is that the Pd+Ni catalysts were more effective than the Pt+Ni catalysts prepared by a similar co-impregnation method, although monometallic Pd catalysts are inferior to monometallic Pt catalysts in oxidative steam reforming of methane.
2. Based on the characterization by the amount of H_2 adsorption and TEM observation, the highest

bed temperature in oxidative steam reforming of methane tends to become higher on the catalysts with larger average metal particle size. In addition, it is concluded that Pd addition is effective for the suppression of temperature increases at the catalyst bed inlet over almost all the Pd-Ni catalysts judging from a comparison with a monometallic Ni catalyst with similar metal particle size. The additive effect of Pd has two aspects: one is that the addition of Pd by the co-impregnation method decreased average metal particle size, and the other is surface modification effect with Pd.

3. The suppression of hot-spot formation in the oxidative steam reforming of methane can be brought about by the enhancement of the reducibility with surface noble metal atoms, thereby causing the overlap between the combustion and the reforming reaction zones. The Pd+Ni catalyst was better than the Pt+Ni catalyst in terms of the suppression of hot-spot formation. Based on the EXAFS analysis, we suggest that the added Pd atoms form small clusters or islands on the bimetallic particle surface, which can be related to surface concentration of Pd being higher than that of Pt.

Acknowledgments

This study was supported by the Industrial Technology Research Grant Program (05A43002C) of the New Energy and Industrial Technology Development Organization (NEDO) of Japan.

References

[1] K. Tomishige, J. Jpn. Petrol. Inst. 50 (2007) 287–298.

[2] K. Tomishige, S. Kanazawa, K. Suzuki, M. Asadullah, M. Sato, K. Ikushima, K. Kunimori, Appl. Catal. A: Gen. 233 (2002) 35–44.

[3] B. Li, K. Maruyama, M. Nurunnabi, K. Kunimori, K. Tomishige, Appl. Catal. A: Gen. 275 (2004) 157–172.

[4] D. Dissanayake, M.P. Rosynek, K.C.C. Kharas, J.H. Lunsford, J. Catal. 132 (1991) 117–127.

[5] B. Li, K. Maruyama, M. Nurunnabi, K. Kunimori, K. Tomishige, Ind. Eng. Chem. Res. 44 (2005) 485–494.

[6] B. Li, R. Watanabe, K. Maruyama, M. Nurunnabi, K. Kunimori K. Tomishige, Appl. Catal. A: Gen. 290 (2005) 36–45.

[7] K. Tomishige, S. Kanazawa, M. Sato, K. Ikushima, K. Kunimori, Catal. Lett. 84 (2002) 69–74.

[8] K. Tomishige, S. Kanazawa, S. Ito, K. Kunimori, Appl. Catal. A: Gen. 244 (2003) 71–82.

[9] B. Li, S. Kado, Y. Mukainakano, M. Nurunnabi, T. Miyao, S. Naito, K. Kunimori, K. Tomishige, Appl. Catal. A: Gen. 304 (2006) 62–71.

[10] B. Li, S. Kado, Y. Mukainakano, T. Miyazawa, T. Miyao, S. Naito, K. Okumura, K. Kunimori, K. Tomishige, J. Catal. 245 (2007) 144–155.

[11] Y. Mukainakano, B. Li, S. Kado, T. Miyazawa, K. Okumura, T. Miyao, S. Naito, K. Kunimori, K. Tomishige, Appl. Catal. A: Gen. 318 (2007) 252–264.

[12] Y. Mukainakano, K. Yoshida, K. Okumura, K. Kunimori, K. Tomishige, Catal. Today 132 (2008) 101–108.

[13] F. Arena, B.A. Horrell, D.L. Cocke, A. Parmaliana, N. Giordano, J. Catal. 132 (1991) 58–67.
[14] K. Tomishige, Y. Himeno, Y. Matsuo, Y. Yoshinaga, K. Fujimoto, Ind. Eng. Chem. Res. 39 (2000) 1891–1897.
[15] K. Tomishige, Y. Chen, K. Fujimoto, J. Catal. 181 (1999) 91–103.
[16] O. Yamazaki, K. Tomishige, K. Fujimoto, Appl. Catal. A: Gen. 136 (1996) 49–56.
[17] D.G. Mustard, C.H. Bartholomew, J. Catal. 67 (1981) 186–206.
[18] J.W. Cook, D.E. Sayers, J. Appl. Phys. 52 (1981) 5024–5031.
[19] K. Okumura, J. Amano, N. Yasunobu, M. Niwa, J. Phys. Chem. B 104 (2000) 1050–1057.
[20] K. Okumura, S. Matsumoto, N. Nishiaki, M. Niwa, Appl. Catal. B: Environ. 40 (2003) 151–159.
[21] A.L. Ankudinov, B. Ravel, J.J. Rehr, S.D. Conradson, Phys. Rev. B 58 (1998) 7565–7576.
[22] B. Li, R. Watanabe, K. Maruyama, M. Nurunnabi, K. Kunimori, K. Tomishige, Catal. Today 104 (2005) 7–17.
[23] R. Ueda, T. Kusakari, K. Tomishige, K. Fujimoto, J. Catal. 194 (2000) 14–22.
[24] K. Tomishige, A. Okabe, K. Fujimoto, Appl. Catal. A: Gen. 194 (2000) 383–393.
[25] S. Takenaka, Y. Shigeta, E. Tanabe, K. Otsuka, J. Phys. Chem. B 108 (2004) 7656–7664.
[26] C. Crisafulli, S. Scirè, R. Maggiore, S. Minicò, S. Galvagno, Catal. Lett. 59 (1999) 21–26.
[27] M. Nurunnabi, Y. Mukainakano, S. Kado, T. Miyao, S. Naito, K. Okumura, K. Kunimori, K. Tomishige, Appl. Catal. A: Gen. 325 (2007) 154–162.
[28] S. Kado, M. Nurunnabi, Y. Mukainakano, T. Miyazawa, K. Nakao, K. Okumura, T. Miyao, S. Naito, K. Suzuki, K. Fujimoto, K. Kunimori, K. Tomishige, ACS Symp. Ser. 959 (2007) 59–72.
[29] M. Nurunnabi, Y. Mukainakano, S. Kado, T. Miyazawa, K. Okumura, T. Miyao, S. Naito, K. Suzuki, K. Fujimoto, K. Kunimori, K. Tomishige, Appl. Catal. A: Gen. 308 (2006) 1–12.
[30] A. Jentys, G.L. Haller, J.A. Lercher, J. Phys. Chem. 97 (1993) 484–488.
[31] Y. Chen, K. Tomishige, K. Yokoyama, K. Fujimoto, Appl. Catal. A: Gen. 165 (1997) 335–347.
[32] J. Nishikawa, T. Miyazawa, K. Nakamura, M. Asadullah, K. Kunimori, K. Tomishige, Catal. Commun. 9 (2008) 195–201.
[33] J. Nishikawa, K. Nakamura, M. Asadullah, T. Miyazawa, K. Kunimori, K. Tomishige, Catal. Today 131 (2008) 146–155.
[34] T.B. Reed, Free Energy Formation of Binary Compounds, MIT Press, Cambridge, 1971.

Table 1 List of catalysts and the properties of reduced catalysts.

Entry	Catalyst [a]	Precursor and loading amount / wt%		Impregnation method [b]	Dispersion [c] / %	Particle size / nm	
		Ni	Pd or Pt	CI or SI	H / (Ni + M) (M = Pd or Pt)	H_2 adsorption [d]	TEM
1	Ni(N, 10.6)	$Ni(NO_3)_2$, 10.6	—	—	3.4±0.3	28	33±2
2	Pd(C, 0.07)	—	$PdCl_2$, 0.07	—	—	.—	—
3	Pd(C, 0.07)+Ni(N, 10.6)	$Ni(NO_3)_2$, 10.6	$PdCl_2$, 0.07	CI	6.6±0.3	15	19±2
4	Pd(A, 0.07)/Ni(N, 10.6)	$Ni(NO_3)_2$, 10.6	$Pd(acac)_2$, 0.07	SI	3.2±0.3	30	36±2
5	Pd(C, 0.07)/Ni(N, 10.6)	$Ni(NO_3)_2$, 10.6	$PdCl_2$, 0.07	SI	3.5±0.3	28	34±2
6	Pd(C, 0.2)+Ni(N, 10.6)	$Ni(NO_3)_2$, 10.6	$PdCl_2$, 0.2	CI	4.3±0.3	23	25±2
7	Pd(A, 0.2)/Ni(N, 10.6)	$Ni(NO_3)_2$, 10.6	$Pd(acac)_2$, 0.2	SI	1.7±0.3	58	53±2
8	Pd(C, 0.2)/Ni(N, 10.6)	$Ni(NO_3)_2$, 10.6	$PdCl_2$, 0.2	SI	2.0±0.3	48	44±2
9	Pt(C, 0.14)	—	H_2PtCl_6, 0.14	—	—	.—	—
10	Pt(C, 0.14)+Ni(N, 10.6)	$Ni(NO_3)_2$, 10.6	H_2PtCl_6, 0.14	CI	4.6±0.3	21	—
11	Pt(A, 0.14)/Ni(N, 10.6)	$Ni(NO_3)_2$, 10.6	$Pt(acac)_2$, 0.14	SI	1.9±0.3	51	—
12	Pt(C, 0.4)+Ni(N, 10.6)	$Ni(NO_3)_2$, 10.6	H_2PtCl_6, 0.4	CI	6.5±0.3	15	19±2
13	Pt(A, 0.4)/Ni(N, 10.6)	$Ni(NO_3)_2$, 10.6	$Pt(acac)_2$, 0.4	SI	3.4±0.3	29	31±2
14	Ni(Ac, 10.6)	$Ni(CH_3COO)_2$, 10.6	—	—	5.3±0.3	18	24±2
15	Ni(C, 10.6)	$NiCl_2$, 10.6	—	—	1.6±0.3	61	58±2

[a] The precursor and the loading amount are denoted in parentheses. N: nitrate, C: chloride, A: acetylacetonate, Ac: acetate. "+": co-impregnation, "/": sequential impregnation.

[b] CI: co-impregnation, SI: sequential impregnation.

[c] Dispersion was determined from H_2 adsorption amount.

[d] Particle size is estimated from 0.971 / Dispersion × 100 assuming that the size of Pd and Pt atoms is the same as that of the Ni atom [13].

Table 2 Catalytic performance in oxidative steam reforming of methane.

Entry	Catalyst	*W*/*F* /g h/mol	CH_4 conversion /%	H_2/CO	CO selectivity /%	Highest bed temperature / K
1	Ni(N, 10.6)	0.04	>99	2.8	81	1349
2	Pd(C, 0.07)	0.23	64	1.9	91	1309
3	Pd(C, 0.07)+Ni(N, 10.6)	0.04	>99	2.8	81	1245
4	Pd(A, 0.07)/Ni(N, 10.6)	0.04	>99	2.8	81	1289
5	Pd(C, 0.07)/Ni(N, 10.6)	0.04	>99	2.9	81	1274
6	Pd(C, 0.2)+Ni(N, 10.6)	0.04	>99	2.9	81	1259
7	Pd(A, 0.2)/Ni(N, 10.6)	0.04	>99	2.8	81	1335
8	Pd(C, 0.2)/Ni(N, 10.6)	0.04	>99	2.9	80	1304
9	Pt(C, 0.14)	0.04	96	2.3	83	1176
10	Pt(C, 0.14)+Ni(N, 10.6)	0.04	>99	2.9	81	1298
11	Pt(A, 0.14)/Ni(N, 10.6)	0.04	>99	2.8	81	1324
12	Pt(C, 0.4)+Ni(N, 10.6)	0.04	>99	2.9	81	1277
13	Pt(A, 0.4)/Ni(N, 10.6)	0.04	>99	3.0	79	1306
14	Ni(Ac, 10.6)	0.04	>99	3.0	80	1326
15	Ni(C, 10.6)	0.04	>99	3.0	78	1379
	Equilibrium	—	>99	2.9	81	—

Reaction conditions: $CH_4/H_2O/O_2/Ar$ = 40/30/20/10; temperature 1123 K; total pressure 0.1 MPa; catalyst weight 0.045 g; H_2 pretreatment at 1123 K

Table 3 Curve fitting results of Pd *K*-edge or Pt L_3-edge EXAFS of the catalysts after the reduction.

Catalyst	Shells	*CN*[a]	*R* /10^{-1} nm[b]	σ /10^{-1} nm[c]	ΔE_0 /eV[d]	R_f / %[e]
Pd(C, 0.2)+Ni(N, 10.6)	Pd-Ni	4.1±0.5	2.53±0.007	0.069±0.006	-4.0±1.6	0.6
	Pd-Pd	5.0±1.0	2.68±0.011	0.069±0.009	2.3±2.0	
Pd(A, 0.2)/Ni(N, 10.6)	Pd-Ni	7.6±0.8	2.53±0.006	0.075±0.004	-1.3±1.4	0.9
	Pd-Pd	2.9±1.9	2.68±0.027	0.076±0.020	9.2±7.6	
Pd(C, 0.2)/Ni(N, 10.6)	Pd-Ni	5.4±0.6	2.53±0.007	0.074±0.005	-3.6±1.5	0.8
	Pd-Pd	4.2±1.4	2.68±0.024	0.075±0.015	7.4±5.6	
Pd foil	Pd-Pd	12.0	2.70	0.060	0.0	
Pt(C, 0.4)+Ni(N, 10.6)	Pt-Ni	8.3±0.6	2.52±0.005	0.065±0.003	4.9±1.1	0.5
	Pt-Pt	1.2±1.0	2.65±0.038	0.065±0.035	4.7±8.8	
Pt foil	Pt-Pt	12.0	2.77	0.060	0.0	

Sample pretreatment: reduction (H_2, 1123 K, 0.5 h).

[a] Coordination number, [b] Bond distance, [c] Debye-Waller factor, [d] Difference in the origin of photoelectron energy between the reference and the sample, [e] Residual factor. Fourier filtering range: 0.169–0.282 nm.

Figure captions

Figure 1 Temperature profiles of the catalyst bed in oxidative steam reforming of methane measured by using an IR thermograph: *W/F* dependence. (A) Ni(N, 10.6), (B) Pd(C, 0.07), (C) Pd(C, 0.07)+Ni(N, 10.6). Reaction conditions: $CH_4/H_2O/O_2/Ar$ = 40/30/20/10; temperature 1123 K; total pressure 0.1 MPa; catalyst weight 0.045 g; H_2 pretreatment at 1123 K.

Figure 2 Reaction time dependence of methane conversion, CO selectivity, and highest bed temperature in oxidative steam reforming of methane over Pd(C, 0.07)+Ni(N, 10.6): Methane conversion (●), CO selectivity (○), Highest bed temperature (△). $CH_4/H_2O/O_2/Ar$ = 40/30/20/10; temperature 1123 K; *W/F* = 0.07 gh/mol; total pressure 0.1 MPa; catalyst weight 0.045 g; H_2 pretreatment at 1123 K.

Figure 3 TEM images of catalysts after H_2 reduction at 1123 K for 0.5 h.
(a) Ni(N, 10.6), (b) Pd(C, 0.2)+Ni(N, 10.6), (c) Pd(A, 0.2)/Ni(N, 10.6), (d) Pt(C, 0.4)+Ni(N, 10.6).

Figure 4 Relation between average particle size and highest bed temperature in oxidative steam reforming.
Average particle size from H_2 adsorption is based on Table 1.
Highest bed temperature in oxidative steam reforming is based on Table 2.

Figure 5 Temperature-programmed reduction profiles of fresh catalysts.
(a) Ni(N, 10.6), (b) Pd(C, 0.2)+Ni(N, 10.6), (c) Pt(C, 0.4)+Ni(N, 10.6), (d) Ni(N, 10.6)-calcined at 773 K again after reduction at 1123 K, (e) Pd(C, 0.2)/Ni(N, 10.6), (e) Ni(N, 10.6)-calcined at 573 K again after reduction at 1123 K and (f) Pd(A, 0.2)/Ni(N, 10.6).
The value in a square bracket means the reduction degree assuming $Ni^{2+} + H_2 \rightarrow 2H^+ + Ni^0$, $Pd^{2+} + H_2 \rightarrow 2H^+ + Pd^0$ and $Pt^{2+} + H_2 \rightarrow 2H^+ + Pt^0$.

Figure 6 Pd *K*-edge EXAFS results of Pd(C, 0.2)+Ni(N, 10.6), Pd(C, 0.2)/Ni(N, 10.6), Pd(A, 0.2)/Ni(C, 10.6) after the H_2 reduction. (A) k^3-weighted EXAFS oscillation, (B) Fourier transform of k^3-weighted EXAFS: FT range: 30–128 nm^{-1}, (C) Fourier filtered EXAFS data (solid line) and calculated data (dotted line): FF range: 0.169–0.282 nm.

(A) Ni(N, 10.6)

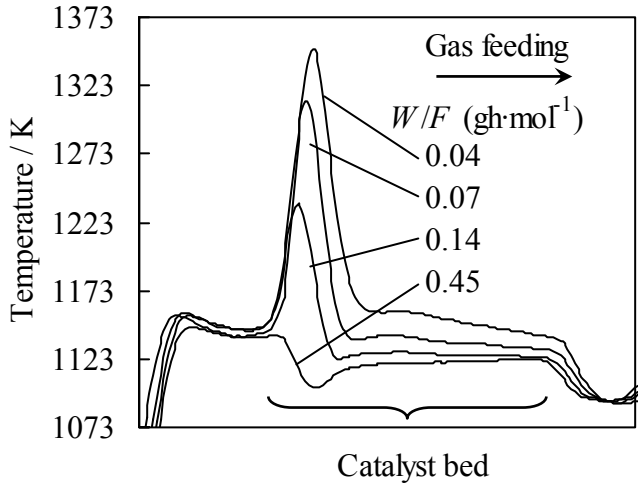

(B) Pd(C, 0.07)

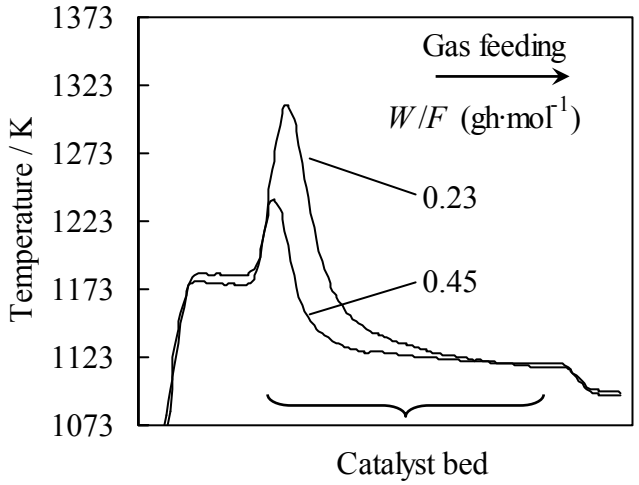

(C) Pd(C, 0.07)+Ni(N, 10.6)

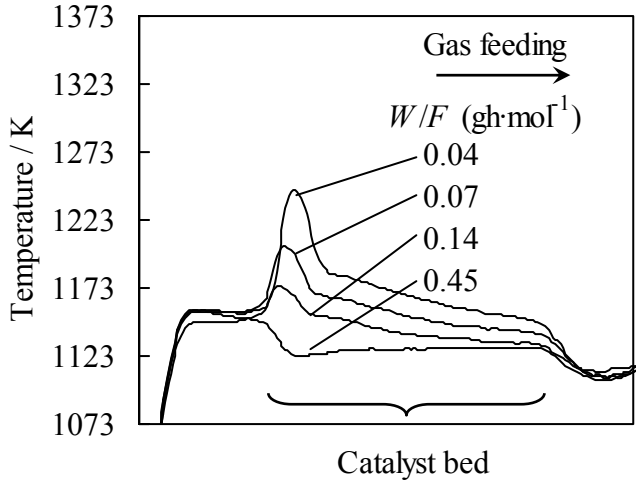

Figure 1 Temperature profiles of the catalyst bed in oxidative steam reforming of methane measured by using an IR thermograph: *W/F* dependence.
(A) Ni(N, 10.6), (B) Pd(C, 0.07), (C) Pd(C, 0.07)+Ni(N, 10.6).
Reaction conditions: $CH_4/H_2O/O_2/Ar$ = 40/30/20/10; temperature 1123 K; total pressure 0.1 MPa; catalyst weight 0.045 g; H_2 pretreatment at 1123 K.

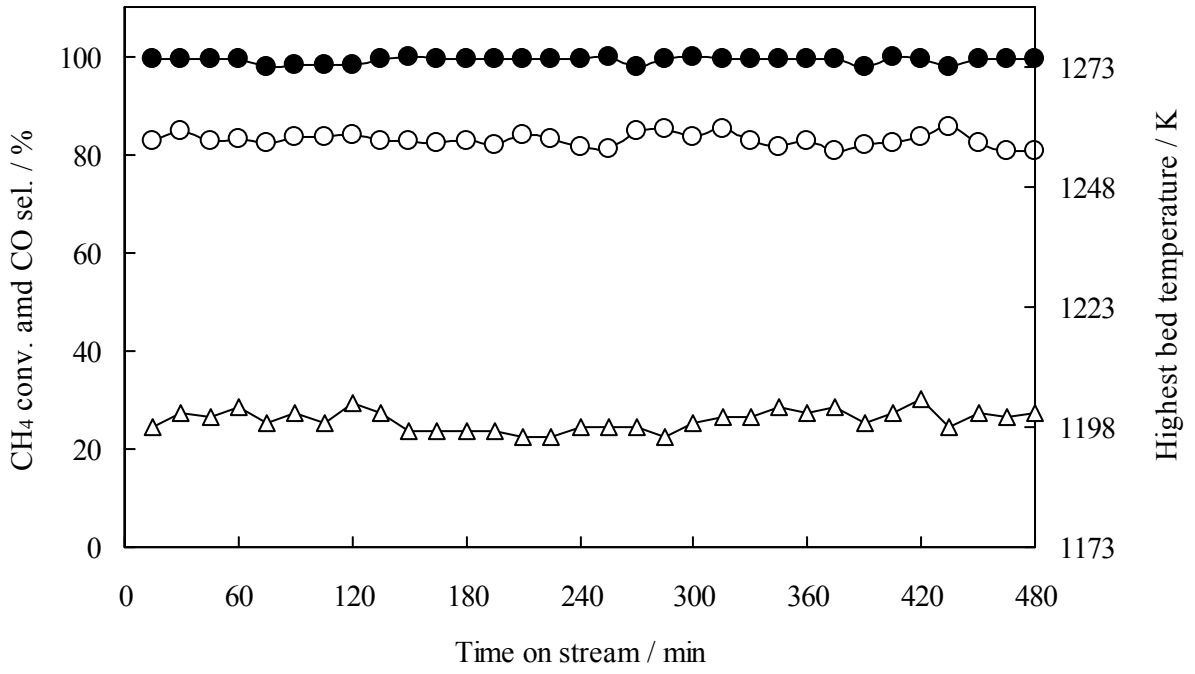

Figure 2 Reaction time dependence of methane conversion, CO selectivity, and highest bed temperature in oxidative steam reforming of methane over Pd(C, 0.07)+Ni(N, 10.6): Methane conversion (●), CO selectivity (○), Highest bed temperature (△). $CH_4/H_2O/O_2/Ar$ = 40/30/20/10; temperature 1123 K; W/F = 0.07 gh/mol; total pressure 0.1 MPa; catalyst weight 0.045 g; H_2 pretreatment at 1123 K.

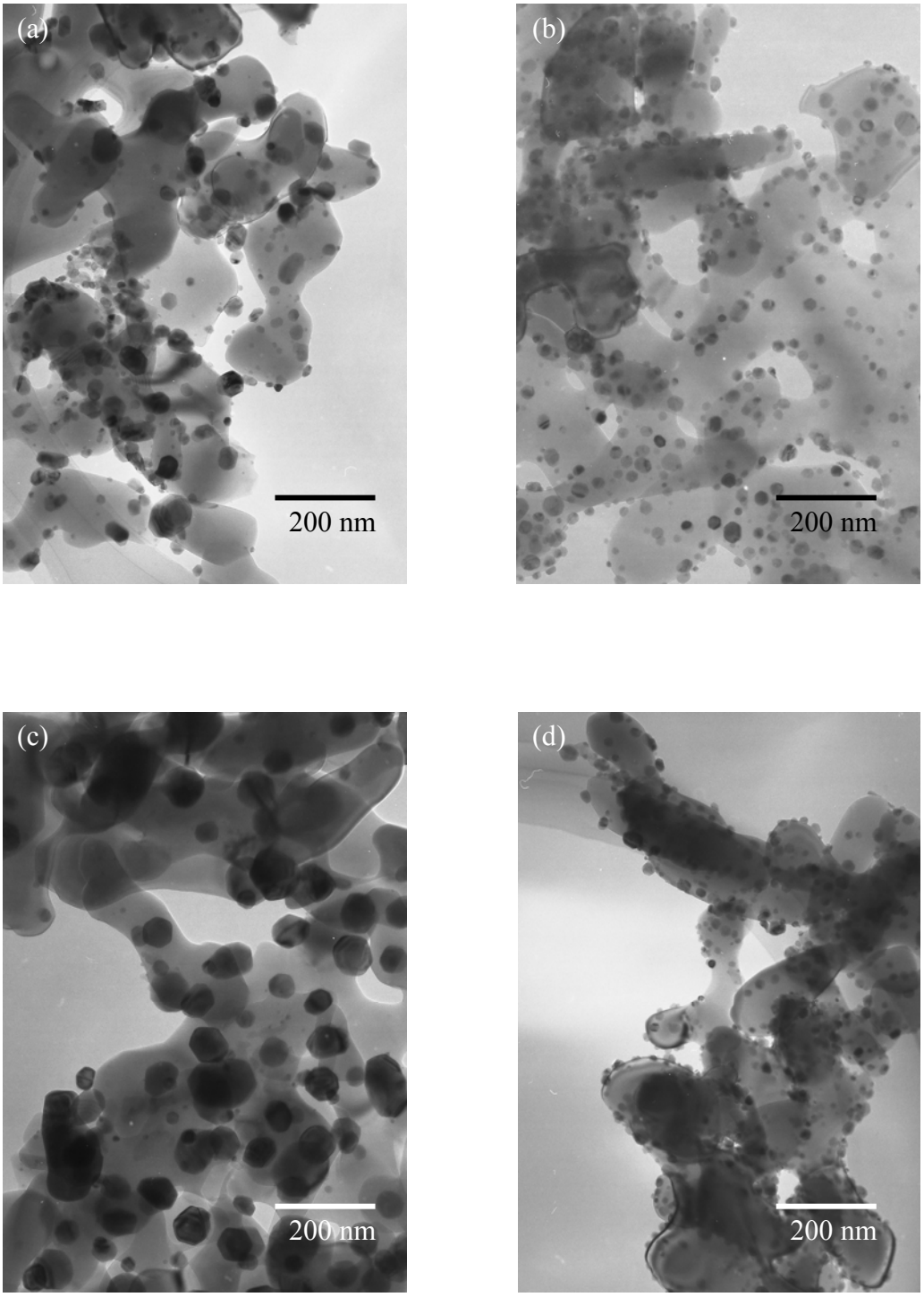

Figure 3 TEM images of catalysts after H_2 reduction at 1123 K for 0.5 h.
(a) Ni(N, 10.6), (b) Pd(C, 0.2)+Ni(N, 10.6), (c) Pd(A, 0.2)/Ni(N, 10.6), (d) Pt(C, 0.4)+Ni(N, 10.6).

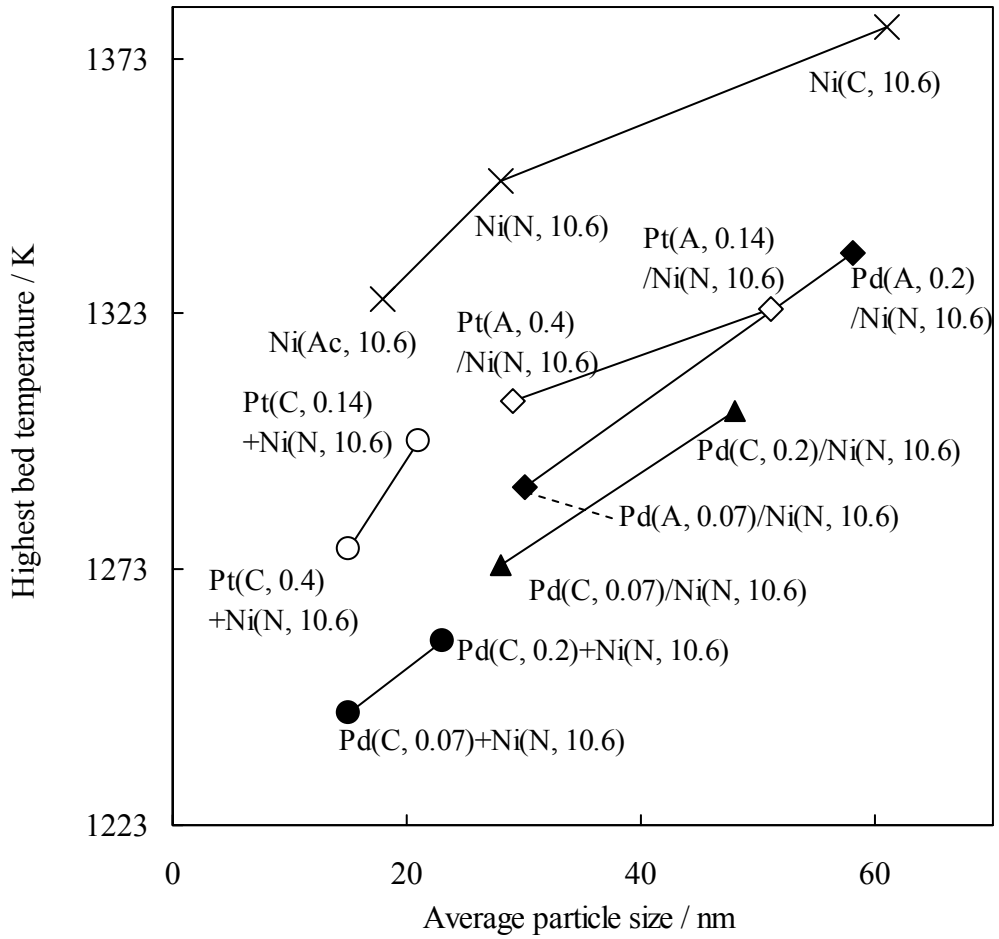

Figure 4　Relation between average particle size and highest bed temperature in oxidative steam reforming.

Average particle size from H_2 adsorption is based on Table 1.

Highest bed temperature in oxidative steam reforming is based on Table 2.

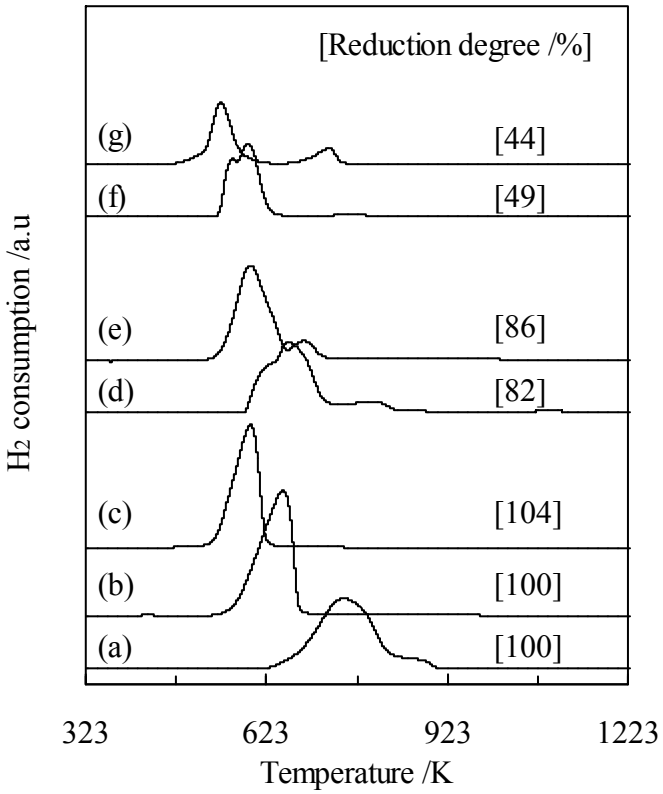

Figure 5 Temperature-programmed reduction profiles of fresh catalysts.
(a) Ni(N, 10.6), (b) Pd(C, 0.2)+Ni(N, 10.6), (c) Pt(C, 0.4)+Ni(N, 10.6), (d) Ni(N, 10.6)-calcined at 773 K again after reduction at 1123 K, (e) Pd(C, 0.2)/Ni(N, 10.6), (e) Ni(N, 10.6)-calcined at 573 K again after reduction at 1123 K and (f) Pd(A, 0.2)/Ni(N, 10.6).
The value in a square bracket means the reduction degree assuming $Ni^{2+} + H_2 \rightarrow 2H^+ + Ni^0$, $Pd^{2+} + H_2 \rightarrow 2H^+ + Pd^0$ and $Pt^{2+} + H_2 \rightarrow 2H^+ + Pt^0$.

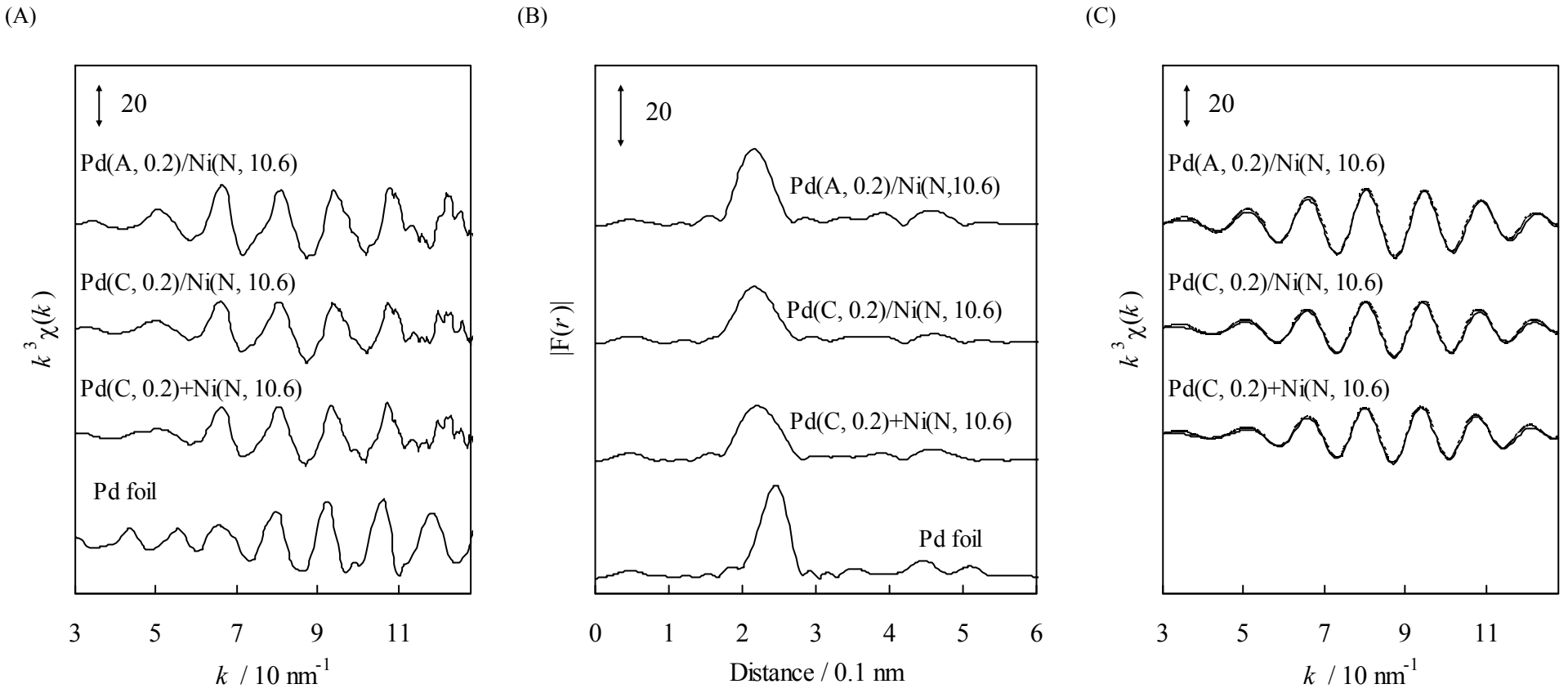

Figure 6 Pd *K*-edge EXAFS results of Pd(C, 0.2)+Ni(N, 10.6), Pd(C, 0.2)/Ni(N, 10.6), Pd(A, 0.2)/Ni(C, 10.6) after the H_2 reduction.
(A) k^3-weighted EXAFS oscillation, (B) Fourier transform of k^3-weighted EXAFS: FT range: 30–128 nm^{-1}, (C) Fourier filtered EXAFS data (solid line) and calculated data (dotted line): FF range: 0.169–0.282 nm.